RSC Advances

ROYAL SOCIETY OF CHEMISTRY

www.rsc.org/advances

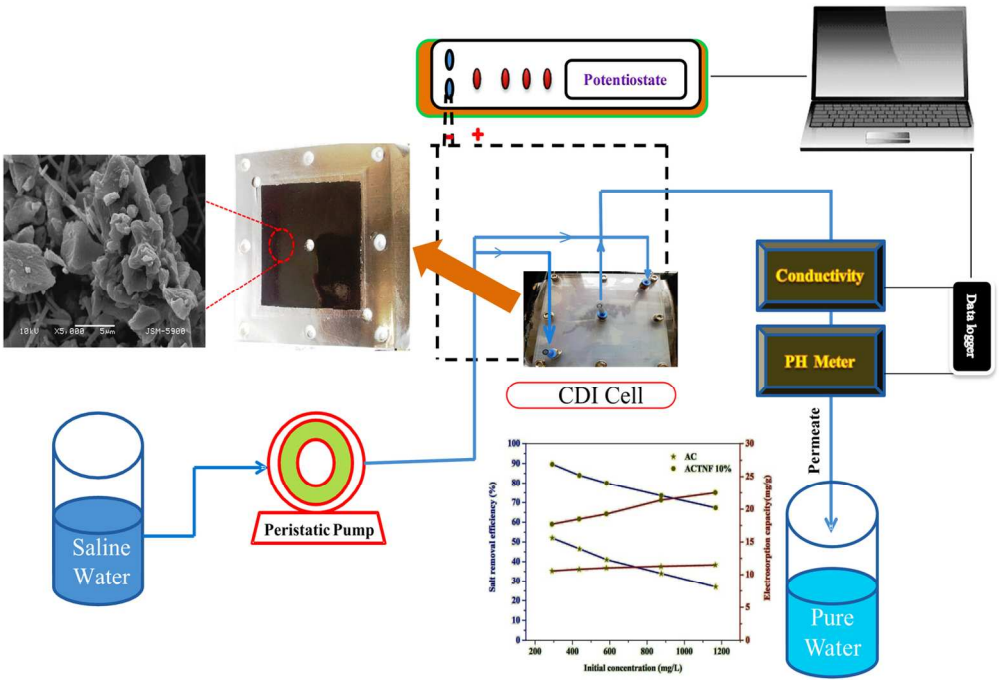

Schematic diagram of capacitive deionization process
133x90mm (300 x 300 DPI)

TiO_2 nanofibers/activated carbon composite as novel effective electrode material for capacitive deionization of brackish water

Ahmed G. El-Deen[1], Jae-Hwan Choi[2], Khalil Abdelrazek Khalil[3,4], Abdulhakim A. Almajid[3] and Nasser A. M. Barakat[1,5,*]

[1]BioNanosystem Department, Chonbuk National University, Jeonju 561-756, South Korea

[2]Department of Chemical Engineering, Kongju National University, 1223-24 Cheonan-daero, Seobuk-gu, Cheonan, Chungnam 331-717, Republic of Korea

[3]Mechanical Engineering Department, King Saud University, P.O. Box 800, Riyadh 11421, Saudi Arabia

[4]Materials Engineering and Design Department, Aswan University, Aswan, Egypt

[5]Chemical Engineering Department, Faculty of Engineering, Minia University, El-Minia, Egypt

Corresponding author:

Nasser A. M. Barakat,

Tel: +82632702363, Fax: +82632702348,

E-mail: *nasser@jbnu.ac.kr*

Abstract

Based on its excellent characteristics, high surface area, environmentally safe and availability in nature; activated carbon (AC) is the best candidate as capacitive deionization (CDI) electrode material. Among various modification methods for AC, incorporation of TiO_2 nanoparticles into the activated carbon showed effective approach to enhance the desalination performance. Compared to nanoparticulate morphology, nanofibers have large axial ratio which provides better electrosorption performance. Herein, for the first time, TiO_2 nanofibers (TNFs) prepared by the electrospinning process were exploited with activated carbon to form hybrid networks electrode for capacitive deionization. The phase morphology and crystal structure were characterized by scanning electron microscopy (SEM) and X-ray diffraction (XRD), respectively. The electrochemical behavior was evaluated by cyclic voltammetry (CV) instrument. Furthermore, the desalination performances under different applied voltages and salty water concentrations were investigated using prototype CDI unit in continuous mode water flow. The results indicated that the electrode prepared from 10 wt% nanofibers (ACTNF 10%) exhibits the best results compared to other electrodes having 5 and 15 wt% TiO_2 nanofibers. Typically, the best electrode networks showed very good specific capacitance (380 F/g), excellent electrosorptive capacity (17.7 mg/g_{carbon}) at cell potential of 1.2V and initial NaCl concentration of 292 mg/L, and distinguished salt removal efficiency (~ 89.6%). Moreover, the introduced electrode shows interesting recyclability and easy full regeneration.

Keywords: TiO_2 Nanofibers/AC; Electrospinning; Capacitive deionization; Water Desalination.

1. Introduction

Fresh water shortage has become one of the greatest dilemmas facing the continuity of the mankind and other creatures in most of the countries. Moreover, contamination of water sources and the dramatic increase in the population **make matters worse** [1]. Consequently, the availability of affordable clean water is the strongest challenges to the international community. Water desalination is a key technology offering an appropriate route to improve the quality and quantity of the pure water [2]. Unfortunately, most of conventional desalination methodologies including multiple-effect distillation (MED), multi-stage flash distillation (MSF), reverse osmosis (RO) and electrodialysis require a great deal of energy, secondary chemical wastes and high capital cost. Hence, developing alternative desalination technologies **are needed** to avoid the drawbacks of the traditional desalination techniques[3, 4]. Capacitive deionization (CDI) is a promising electrosorption technology to desalinate brackish water; it has been recently attracting unprecedented attention in desalination field due to the power saving, eco-friendly and easily operational and maintenance processes[5-9]. CDI, in essence, is a purely capacitive process based on the principle of electrosorption of ions on charged pours electrodes formed by the electrical double layer (EDL). Electrostatically, the adsorbed ions may be either released from the electrode pore surfaces by shunting the electrodes together, or, at least in the membrane version, may be actively driven off by reversing polarity[10, 11]. A problem with capacitive deionization is the concentration polarization of the electrodes. This kind of polarization refers to a depletion of ions at the electrode surface. This has deleterious effects, such as an increased resistance. Therefore, reducing the concentration polarization of the capacitive carbons is important to attaining improved performance, not only for capacitive deionization, but for electric double

layer capacitors (ELDC's) in general. Methods which increase surface wettability are expected to be important in this regard.

Typically, high surface area, good chemical inertia, wettability characteristics, excellent electrochemical performance as well as low electric polarization are the most important features for optimum CDI electrode material[12, 13]. In fulfilling the foregoing requirements, carbon materials are the best candidates as CDI electrode. Recently, porous carbon materials such as carbon aerogels[14], macro and mesoporous carbon (MC)[15-18], multi-channels and hollow carbon nanofibers[19-21],carbon nanotube[22-24] and graphene composite[25-30] have been investigated as electrode materials. However, up to date, activated carbon (AC) is a commonly used as porous CDI electrode material because of its great surface area with a high degree of porosity and exceptional adsorption capability as well as low cost[31]. Unfortunately, the AC electrodes are polarisable. As well known, the polarization reduces accumulation of ions on the double-layer of AC [32]. A recent, surprising development regarding surface modification of the carbon electrodes for capacitive deionization is the discovery that ionic group molecules incorporated within the Debye length region of the double layer volume of the electrode pores polarize the electrodes with respect to anions or cations. This achieves coulombic efficiency without use of membranes. Coulombic efficiency is necessary to achieve better purification, water, and energy efficiency[33, 34].

Among various metal oxides, TiO_2 is a low cost, eco-friendly and having known photocatalytic ability for degradation of the organic pollutants and annihilation of some microorganisms. Moreover, its good charged surface leads to reduce the polaization of AC thereby the electrosorption capacity could be increased[35, 36]. The aggregation of TiO_2 nanoparticles (NPs) is a severe dilemma negatively affects the performance of conventional TiO_2

NPs/AC electrodes[37, 38]. In other words, most of reported methods for modified AC by TiO_2 nano or microparticles still can't prevent agglomeration process and pore blocking of the electrode surface. Among the reported nanostructures, nanofibrous morphology has a large axial ratio that leads to prevent intra aggregation and inter agglomeration in TiO_2 nanofibers/AC composite (ACTNF). Hence, using TiO_2 nanofibers with AC as CDI electrode is expected to increase the accessibility for ion adsorption, and accelerate ions diffusion pathway form saline solution to surface electrode.

In this study, the TiO_2 nanofibers intercalated AC (ACTNF) as hybrid network CDI electrode is introduced. To evaluate the desalination behavior of the modified AC electrode, the proposed composite electrode was investigated under different factors during CDI process. It is noteworthy, this network composite achieved a lot of electrode requirements; cost-effective, good wettability, decrease polarization of the surface, prevent agglomerations process and easy regeneration.

2. Experimental

2.1. Materials

Titanium (IV) isopropoxide ($C_{12}H_{28}O_4Ti$, 98.0 assay), Poly (vinyl acetate) (PVAc, MW = 500,000 g/mol) was obtained from Aldrich, USA. N, N-dimethylformamide (DMF 99.5% assay; SAMCHUN Pure Chemical Co., South Korea), activated carbon powder (CEP-21K, PCT Co., Korea, BET surface area = 1320 m^2/g), poly (vinylidene fluoride) (PVdF, M.W. = 530,000, Aldrich) and dimethylacetamide (DMAc, Aldrich). All reagents were used without any further purification.

2.2. Synthesis TiO_2 nanofibers by electrospinning.

The TiO_2 nanofibers were synthesized by electrospinning technique[39]. In detail, 1 g titanium isopropoxide $Ti(OiPr)_4$ was added to 2 g poly(vinyl acetate) (PVAc, 14 wt% in DMF) then few drops of acetic acid were added until the solution became transparent, the mixture was stirred at 25 °C for 2h to form sol gel. Electrospinning of the sol gel solutions was carried out at 20 kV and 18 cm distance between the collector and the tip of the syringe. The obtained electrospun nanofiber mats were initially dried for 24 h at 60 °C in a vacuum and then sintered in air atmosphere at 700 °C for 1 h with a heating rate of 5 °C/min.

2.3. Fabrication of Activated carbon/TiO_2 nanofibers nanocomposite electrodes

To fabricated ACTNF networks CDI electrode, specific amount of the obtained TNFs (5 wt% ,10wt% and 15 wt%) were combined with dispersion solution of AC in DMAC then the mixture was sonicated for 1h, the sol-gel of polyvinylidene fluoride (PVDF, 10 wt%) dissolved in DMAC was added as a binder. The mixture transferred into high speed mixer (AR-100, THINKY Co., Japan) for 20 min at 20000 rpm to ensure homogeneity. The obtained slurry was casted onto graphite foil (F02511, Dongbang Carbon Co., Korea) using a doctor blade (the thickness nanocomposite electrode material was ~ 250 μm). The final electrode was dried at under vacuum at 60 °C for 2 h to remove all organic solvent. The electrode area was maintained as 10×10 cm^2 active area (100 cm^2).

2.4 Characterization

The surface morphology was studied by a JEOL JSM-5900 scanning electron microscope (JEOLLtd., Japan) and field-emission scanning electron microscope (FESEM Hitachi S-7400, Japan). The phase and crystallinity were characterized using Rigaku X-ray diffractometer (XRD, Rigaku Co., Japan) with Cu Kα (λ = 1.54056 Å) radiation over a range of 2θ angles from 10 to 70^{o}. Cyclic voltammetry measurement was carried out using different concentrations (0.1, 0.5 and 1 M) NaCl solutions, the sweep potential rang was adjusted from -0.4 to 0.6 V in an electrochemical cell with three-electrode system: platinum wire as counter electrode, Ag/AgCl as reference electrode and the prepared materials as working electrode. This system was controlled using VersaStat4 potentiostat device. Herein, the specific capacity was calculated by integrating the area of the CV curve to determine the average value according to the following equation [40, 41].

$$Cs = \frac{\int I \mathrm{d}V}{2v\Delta V m} \quad \textbf{(1)}$$

Where *C*s is the specific capacitance (F/g), *I* is the current (A), *v* is the scan rate (V/s), ΔV is the applied potential window (V), and *m* is the mass of active electrode materials (g).

2.5 CDI unit cell setup and electrosorptive capacity measurements.

Capacitive deionization system consisting of a reservoir, peristaltic pump, potentiostat (WPG100, WonA Tech Co., Korea), CDI cell, conductivity meter (Model ET901, eDAQ) and pH meter was utilized; Fig 1 displays the used system setup. The CDI unit cell composed of two parallel electrode sheets separated by a non-conductive spacer (nylon cloth, 100 μm thick) and fixed with rubber gasket [42]. The saline solution (influent) was continuously pumped into the CDI

cell with 20 ml/min and the initial conductivity was approximately 560μS/cm using single-pass experiment (SP-method). The different potentials (0.8-2.0 V) were applied in the CDI cell to study the desalination performance. The salt removal efficiency (η_d) and the electrosorption capacity (Q) of the electrode could be examined by the salt concentration change during the adsorption process[43, 44]:

$$\eta_d = 1 - \left(\frac{C_{\mathrm{avr}}}{C\mathrm{o}}\right) \times 100 \quad \textbf{(2)}$$

$$Q = \frac{(C\mathrm{o} - C_{\mathrm{avr}})\, V}{M} \quad \textbf{(3)}$$

Where $C\mathrm{o}$ (mg/L) is the initial NaCl concentration, C_{avr} is the average NaCl concentration of the effluent during the adsorption process and V (L) is the total volume of the NaCl aqueous solutions, and M (g) represents the mass of active electrode materials.

3. Results and discussion

3.1 Phase morphology

Electrospinning has been recognized as an efficient technique for the fabrication of nanofibers structure. Electrospun fibers can adopt the diameter and porous morphology undergoes natural polymer composited and directing polymer solution from syringe nozzle design[45]. Accordingly,

good nanofibers morphology is expected from the electrospinning process. Figure 2A depicts SEM image of the fabricated PVAc/$Ti(OiPr)_4$ electrospun mats after drying under vacuum at 60 ^oC for 24h. Clearly, the results reveal good morphology nanofibers without beads. After calcination, the obtained powder demonstrates smooth and good continuous nanofibrous morphology as shown in Fig 2B. It is noteworthy, the diameter frequency charts have been determined for the electrospun mat and the final TiO_2 nanofibers and displayed as the insets Fig. 2 A and B, respectively. From the obtained data, the average diameters were estimated to be 437 and 352 nm for electrospun mat and TiO_2 nanofibers, respectively. Figure 2C displays the microstructure of the utilized activated carbon. Panel 2D displays the low magnification SEM images for ACTNF10% hybrids networks; the inset is a high magnification display. Obviously, the TiO_2 nanofibers intercalated into activated carbon to form networks structure that leads to reduce the particles agglomeration furthermore avoid clogging pores of the activated carbon. Moreover, Fig S1 in supporting information shows the SEM image of ACTNFs 5% and ACTNFs 15% composite electrode. As shown, the surface of ACTNFs electrode having 15 wt% was almost coated by TiO_2 NFs. Energy dispersive X-ray spectroscopy (EDX) spectrum in Fig. 2E conforms the presence of C, Ti and O elements in the investigated area and the inset table shows the atomic and weight ratios.

The XRD analysis technique is widely employed to identify the crystallographic structures for the fabricated materials. Fig. 3 shows XRD spectra of pristine AC, pure TiO_2 NFs and ACTNF 10%. AC reveals two very weak broad characteristic peaks positioned at $2\theta = 24.1°$ and 43.3° corresponding to diffraction from (002) and (100) crystal planes of graphite, respectively. The broad diffraction peaks reflect a highly disordered and amorphous framework of the utilized

activated carbon. The middle spectrum reveals the distinctive peaks corresponding to (101), (004), (200), (105), and (211) for pure anatase TiO_2 NFs. On the other hand, the ACTNF 10% composite exhibits similar diffraction peaks of TiO_2 indicating the TiO_2 NFs incorporated into AC.

3.2 Surface wettability test

To investigate the surface characteristics for the fabricated electrode materials, static contact angles were measured from the water drop on the fabricated electrode at room temperature. As shown in Fig 4, the static contact angle of a water droplet for pristine AC was approximately 129.7°. On the other hand, the ACTNF 10% composite electrode displays a noticeable decrease in contact angel ~77.53°. Consequently, the incorporated TiO_2 nanofibers into AC electrode revealed a marked improvement in the surface wettability due to the hydrophilicity of TiO_2. The most important finding, the designed TiO_2 nanofibers in the ACTNF 10% electrode revealed good wettability behavior without pore blocking that leads to enhance the adsorption rate from the saline solution to the electrode surface more than coating method.

3.3 Electrochemical behavior

Cyclic voltammetry (CV) measurements are often applied as effective tools to investigate the electrosorption behavior and evaluate the specific capacitance of the fabricated electrodes materials. Fig. 5A shows the CV profiles of the AC and ACTNF (5%, 10% and 15%) composite electrodes at a scan rate of 10 mV/s in a 1 M NaCl aqueous solution. Obviously, in all formulations, there are no observed redox peaks during the measurement indicates that the ions

are adsorbed on the electrode surface by forming an electric double layer due to Coulombic interaction rather than electrochemical reaction. Furthermore, the obtained rectangular shape implies excellent electrochemical double-layer capacitance behavior [46]. Moreover, the impact of TiO_2 loading on electrosorption behavior can be observed in Fig 5A. The ACTNF (10% wt TiO_2 NFs) electrode demonstrates the largest encircled area under CV curve indicating higher and distinguished electrochemical performances. However, the ACTNF 15wt% shows significant loss in EDL capacitance which can be attributed to the blockage of the pores of AC electrode and increasing in the contact resistance between AC and TNFs compared to ACTNF 10 wt%. Fig 5B displays CV curves of ACTNF10% electrode at different scan rates in 1M NaCl. As shown, gradual change from ideal rectangular shapes to oval shapes can be observed which can be attributed to the inherent resistivity of the salt solutions as well as the electrode polarization[47]. Another interesting finding can be observed from Fig. 5C, with increasing concentration, the CV curve inclined to typical rectangular shape and the circulated area became wider indicating large amount of salt ions can be electrostatically adsorbed as well as high corresponding specific capacitance. It should be worthwhile noting that this result demonstrates an excellent reversible ion adsorption/desorption capability due to the uniform network distribution of TiO_2 nanofibers between AC particles without cover the active pore site of AC.

The specific capacitances have been calculated from I-V cycles based on Eq. 1. It well known that, a lower scan rate is desirable for the electrosorption capacitance because of high accessibility to accumulate the ions on the electrode surface. Fig. 6A displays the corresponding specific capacitance plot for the synthesized electrode materials versus scan rates. Obviously, the ACTNF10% revealed a significant increase compared to the other fabricated electrodes. Typically, at 10 mV/s scan rate, the specific capacitances are determined to be 219, 349.6, 380 and 111 F/g for AC, ACTNF 5%, 10% and 15%, respectively (Fig S2 in supporting information).

Herein, the optimum ratio for TNFs intercalated into AC hybrid CDI electrode is 10wt%. Although the overloading of the incorporated TNFs into AC electrode can enhance the surface wettability based on hydrophilicity of TiO_2, it has negative impact on electrochemical capacitance behavior due to increase the internal resistance [48]. Based on hydrophilicity of TiO_2, increasing of TiO_2 content on AC leads to enhance the wettability behavior of composite electrode. Although TiO_2 itself has very low capacitance, incorporating of TiO_2 into carbon materials can enhance the capacitance of the composite due to the interaction between carbon and TiO_2 and surface polarization. On the other hand, with increasing of the TiO_2 content in composite, the electrochemical capacitance decreased due to the following phenomena: (i) the further decrease in polarization, and (ii) increase of the contact resistance between AC and TiO_2. Cycle lifetime of the ACTNFs 10% as active material was examined at scan rate of 10 mV/s for 50 cycles and the capacitance retention was calculated for each cycle as shown in Fig 6B. Obviously, neglected decrease in the electrochemical capacitance can be observed as the capacitance retention maintained at ~98.9% over 50 successive cycles which evidenced their excellent cycle stabilities.

3.4. Desalination performance and electrosorption capacity

Single pass mode experiments were conducted in NaCl aqueous solution during adsorption and desorption process, the electrosorption behavior of the fabricated ACTNF 10% networks and AC electrodes were studied under various conditions. The typical condition of desalination experiment was conducted in NaCl solution with an initial conductivity ~ 560 µS/cm and 20ml/min as flow rate. The change in conductivity of effluent during adsorption/desorption process under cell potential of 1.2V was depicted in Fig 7A. Obviously, a sharp decrease in the conductivity reflects significant variation in the NaCl concentration during

charge step corresponding to the ability of the introduced material towards ionic adsorption process in CDI cell. With time going, the rate of the adsorption of ions represented in conductivity curve becomes slowly because of saturation of the adsorption capacity of the electrode [49]. As shown in the figure, the ACTNF10% network electrode declined the conductivity from 560 to 58 μS/cm however it decreased from 560 to 272 μS/cm in case of utilizing pristine AC electrode reflects noticeable improvement in desalination efficiency during the CDI process under same condition. It is worth mentioning, the sharp increase in conductivity at desorption stage corresponds to the expulsion of ions adsorbed at reverse current under 0V. This indicates that desorption proceeded of ACTNF 10% electrode is faster and easier than pristine AC. This excellent deionization capacity for the ACTNF10% electrode can be attributed to decreasing the electric polarization of the AC and increasing the wettability by anchoring of TiO_2. Moreover, designed of TiO_2 nanofiber structure provides rapid and easily adsorption of the ions through intra-channel pathway on electrode surface.

Regeneration behavior is the most important factor for evaluating the cost and lifetime efficiency of the CDI electrode. Fig 7B displays successive adsorption/desorption processes for AC and the modified ACTNF 10% hybrid electrode. Apparently, the ACTNF 10% demonstrated high stability of adsorption capacity during four consecutive cycles. Moreover, a great similarity in the cycle's profiles can be observed which indicates full regeneration during the adsorption processes. Generally, the applied voltage is the key factor to the CDI efficiency. Consequently, the desalination performance for the ACTNF 10% electrodes under different cell potentials from 0.8 to 2.0 V were investigated. As shown in Fig. 8A, the CDI profile for multi consecutive cycles versus applied potential confirmed an increase in the desalination performance. By applying Eq.

2 and 3, the salt removal efficiency and electrosorptive capacity were calculated and plotted versus the applied voltages in Fig. 8B. Typically, the adsorption capacity of both electrode increases with increasing the applied voltage. However, The ACTNF 10% demonstrated significant outweigh on AC pure electrode under all applied voltages. Influence of NaCl concentration as an important indication to evaluate full performance of CDI electrode materials was also studied. Fig. 9 displays the salt removal efficiency and electrosorption capacity for proposed electrodes during CDI process as a function of NaCl concentration solution. The decline in desalination ratio can be attributed to the saturation of electrode surface with increasing the initial NaCl concentration. Interestingly, the ACTNFs 10% electrode achieved 143% increase in the desalination ratio; more than double times of electrosorption capacity at 1200 mg/L initial NaCl concentration compared to pure AC. Based on all of the foregoing results, the ACTNF 10% networks electrode has significantly outweigh throughout CDI measurements compared to original AC. It should be noted that, the salt removal efficiency and electrosorption capacity of the TiO_2 nanofibers intercalated into AC to form ACTNF 10% networks electrode outperforms most efficient titania-doped AC CDI electrode which were recently reported are summarized in Table 1 for comparison; as shown the introduced electrode is superior.

Conclusion

Hybrid networks CDI electrode can be fabricated by intercalating TiO_2 nanofibers into AC. Compared to surface modification methods of AC, the incorporating of TiO_2 nanofibers structured into AC submitted a remarkable increase for the desalination performance. The

distinct performance can be attributed to unique designed of the nanofibrous morphology that avoids blocking pores surface of AC and open interfacial pathway between AC particles to increase the adsorption rate of ions from salt solution to electrode surface. Additionally, the amount of incorporated TiO_2 should be optimized to achieve the highest desalination efficiency; 10 wt% is the recommended percentage. The proposed ACTNF 10% network electrode has a good surface wettability, superiority in electrochemical behaviour, excellent desalination efficiency moreover complete regeneration. Hence, the introduced ACTNF 10% can be successfully utilized as electrodes in capacitive deionization system.

Acknowledgment

The Authors extend their appreciation to the Deanship of Scientific Research at King Saud University for funding the work through the research group project No. IRG14-11.

References

1. M. A. Shannon, P. W. Bohn, M. Elimelech, J. G. Georgiadis, B. J. Mariñas and A. M. Mayes, *Nature*, 2008, **452**, 301-310.
2. M. Schiffler, *Desalination*, 2004, **165**, 1-9.
3. M. Elimelech and W. A. Phillip, *Science*, 2011, **333**, 712-717.
4. T. Hillie and M. Hlophe, *Nature Nanotechnology*, 2007, **2**, 663-664.
5. S. Porada, R. Zhao, A. Van Der Wal, V. Presser and P. Biesheuvel, *Prog. Mater Sci.*, 2013, **58**, 1388-1442.
6. T. Welgemoed and C. Schutte, *Desalination*, 2005, **183**, 327-340.
7. Y. Oren, *Desalination*, 2008, **228**, 10-29.
8. O. N. Demirer, R. M. Naylor, C. A. Rios Perez, E. Wilkes and C. Hidrovo, *Desalination*, 2013, **314**, 130-138.
9. M. A. Anderson, A. L. Cudero and J. Palma, *Electrochim. Acta*, 2010, **55**, 3845-3856.
10. F. A. AlMarzooqi, A. A. Al Ghaferi, I. Saadat and N. Hilal, *Desalination*, 2014, **342**, 3-15.
11. C. A. R. Perez, O. N. Demirer, R. L. Clifton, R. M. Naylor and C. H. Hidrovo, *J. Electrochem. Soc.*, 2013, **160**, E13-E21.
12. B. P. Jia and L. D. Zou, *Chem. Phys. Lett.*, 2012, **548**, 23-28.
13. W. Huang, Y. Zhang, S. Bao and S. Song, *Surf. Rev. Lett.*, 2013, **20**.
14. J. C. Farmer, D. V. Fix, G. V. Mack, R. W. Pekala and J. F. Poco, *J. Electrochem. Soc.*, 1996, **143**, 159-169.
15. C. Tsouris, R. Mayes, J. Kiggans, K. Sharma, S. Yiacoumi, D. DePaoli and S. Dai, *Environ Sci Technol*, 2011, **45**, 10243-10249.
16. S. Porada, L. Weinstein, R. Dash, A. Van der Wal, M. Bryjak, Y. Gogotsi and P. Biesheuvel, *ACS applied materials & interfaces*, 2012, **4**, 1194-1199.
17. Z. Peng, D. Zhang, L. Shi, T. Yan, S. Yuan, H. Li, R. Gao and J. Fang, *The Journal of Physical Chemistry C*, 2011, **115**, 17068-17076.
18. J. Yang and L. Zou, *Microporous Mesoporous Mater.*, 2014, **183**, 91-98.
19. A. El Deen, K. Khalil, N. Barakat and K. H. Yong, *J. Mater. Chem. A*, 2013, **1**, 11001-11010.
20. A. G. El-Deen, N. A. Barakat, K. A. Khalil and H. Y. Kim, *New J. Chem.*, 2014, **38**, 198-205.
21. Q. Dong, G. Wang, B. Qian, C. Hu, Y. Wang and J. Qiu, *Electrochim. Acta*, 2014, **137**, 388-394.
22. Y. Liu, H. Li, C. Nie, L. Pan and Z. Sun, *Desalination and Water Treatment*, 2013, 1-7.
23. D. S. Zhang, T. T. Yan, L. Y. Shi, Z. Peng, X. R. Wen and J. P. Zhang, *J. Mater. Chem.*, 2012, **22**, 14696-14704.
24. Z. Peng, D. Zhang, T. Yan, J. Zhang and L. Shi, *Appl. Surf. Sci.*, 2013, **282**, 965-973.
25. A. G. El-Deen, N. A. M. Barakat and H. Y. Kim, *Desalination*, 2014, **344**, 289-298.
26. H. Li, L. Zou, L. Pan and Z. Sun, *Environ Sci Technol*, 2010, **44**, 8692-8697.
27. X. Wen, D. Zhang, T. Yan, J. Zhang and L. Shi, *Journal of Materials Chemistry A*, 2013, **1**, 12334-12344.
28. X. Wen, D. Zhang, L. Shi, T. Yan, H. Wang and J. Zhang, *J. Mater. Chem.*, 2012, **22**, 23835-23844.
29. H. Li, S. Liang, J. Li and L. He, *Journal of Materials Chemistry A*, 2013, **1**, 6335-6341.
30. A. G. El-Deen, N. A. Barakat, K. A. Khalil, M. Motlak and H. Yong Kim, *Ceram. Int.*, 2014.
31. L. Zou, G. Morris and D. Qi, *Desalination*, 2008, **225**, 329-340.
32. D. Qu, *J. Power Sources*, 2002, **109**, 403-411.
33. M. Andelman, *Journal of Materials Science and Chemical Engineering*, 2014, **2014**.
34. M. D. Andelman, Google Patents, Editon edn., 2012.
35. L. Lu, Y. Zhu, F. Li, W. Zhuang, K. Y. Chan and X. Lu, *J. Mater. Chem.*, 2010, **20**, 7645-7651.

36. M.-K. Seo and S.-J. Park, *Current Applied Physics*, 2010, **10**, 391-394.
37. P.-I. Liu, L.-C. Chung, H. Shao, T.-M. Liang, R.-Y. Horng, C.-C. M. Ma and M.-C. Chang, *Electrochim. Acta*, 2013, **96**, 173-179.
38. C. Kim, J. Lee, S. Kim and J. Yoon, *Desalination*, 2014, **342**, 70-74.
39. M. Motlak, M. S. Akhtar, N. A. Barakat, A. Hamza, O. Yang and H. Y. Kim, *Electrochim. Acta*, 2014, **115**, 493-498.
40. X. Ning, W. Zhong, S. Li, Y. Wang and W. Yang, *Journal of Materials Chemistry A*, 2014, **2**, 8859-8867.
41. N. A. Barakat, A. G. El-Deen, G. Shin, M. Park and H. Y. Kim, *Mater. Lett.*, 2013, **99**, 168-171.
42. J.-H. Lee, W.-S. Bae and J.-H. Choi, *Desalination*, 2010, **258**, 159-163.
43. L. Li, L. Zou, H. Song and G. Morris, *Carbon*, 2009, **47**, 775-781.
44. Y.-J. Kim and J.-H. Choi, *Water Res.*, 2010, **44**, 990-996.
45. Z.-M. Huang, Y.-Z. Zhang, M. Kotaki and S. Ramakrishna, *Compos. Sci. Technol.*, 2003, **63**, 2223-2253.
46. G. Wang, L. Zhang and J. Zhang, *Chem. Soc. Rev.*, 2012, **41**, 797-828.
47. H. Wang, D. Zhang, T. Yan, X. Wen, L. Shi and J. Zhang, *J. Mater. Chem.*, 2012, **22**, 23745-23748.
48. H. Liang, F. Chen, R. Li, L. Wang and Z. Deng, *Electrochim. Acta*, 2004, **49**, 3463-3467.
49. B. Jia and L. Zou, *Carbon*, 2012, **50**, 2315-2321.
50. L. Zou, L. Li, H. Song and G. Morris, *Water Res.*, 2008, **42**, 2340-2348.
51. H.-I. K. Jeong-Won Lee, Han-Joo Kim, and Soo-Gil Park, *Applied Chemistry for Engineering*, 2010, **21**, 265-271.
52. H. Yin, S. Zhao, J. Wan, H. Tang, L. Chang, L. He, H. Zhao, Y. Gao and Z. Tang, *Adv. Mater.*, 2013, **25**, 6270-6276.

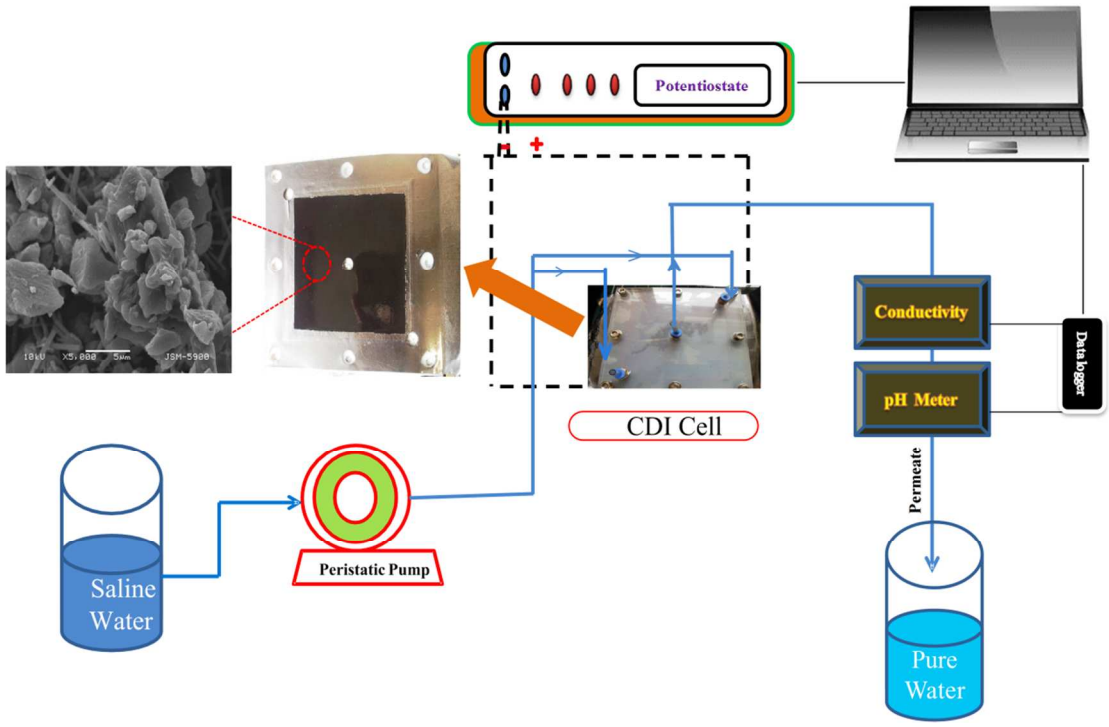

Fig. 1 Schematic diagram of capacitive deionization process

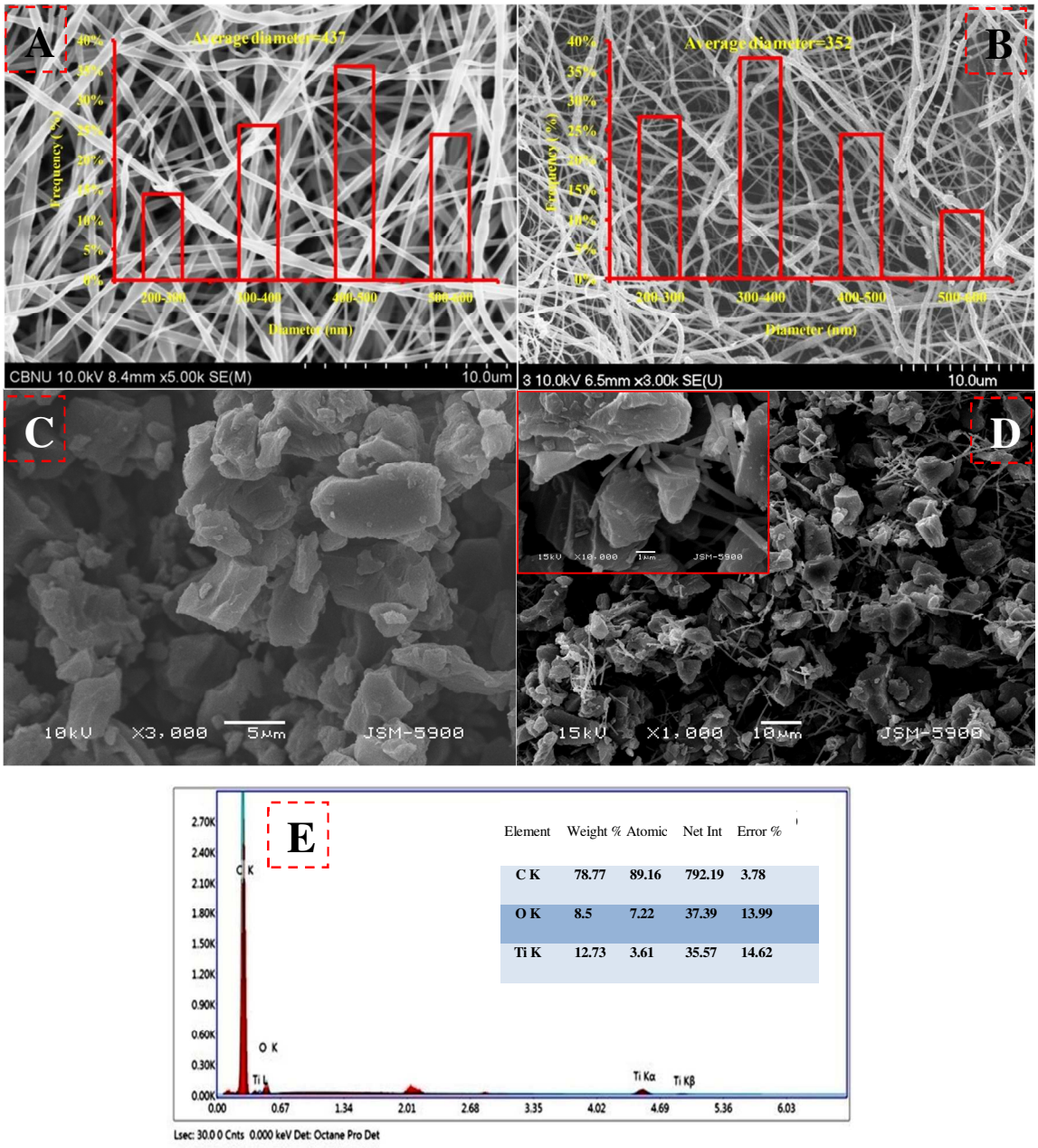

Element	Weight %	Atomic	Net Int	Error %
C K	78.77	89.16	792.19	3.78
O K	8.5	7.22	37.39	13.99
Ti K	12.73	3.61	35.57	14.62

Fig. 2 (A, B) SEM images of PVAc/Ti(OiPr)$_4$ electrospun nanofiber mat and pure TiO_2 nanofibers after calcination, pristine activated carbon (C), SEM images of the ACTNF 10% and inset is high magnification (D) and EDX analysis for the ACTNF 10% electrode (E)

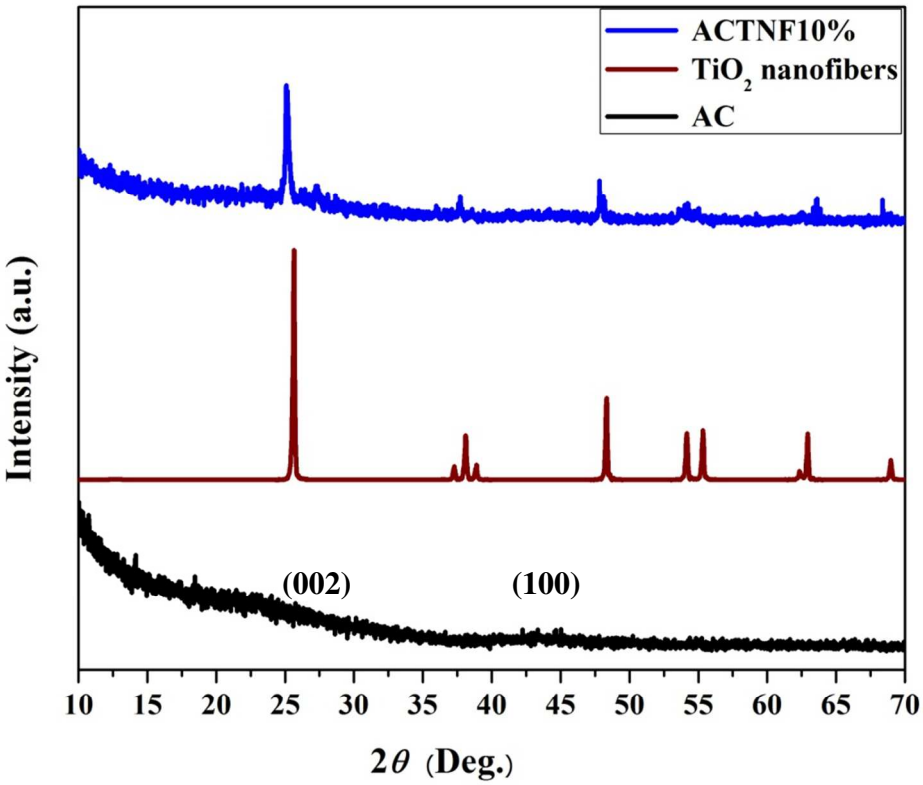

Fig. 3 XRD patterns for the fabricated electrode materials; pristine AC, Pure TiO_2NFs and ACTNF10%

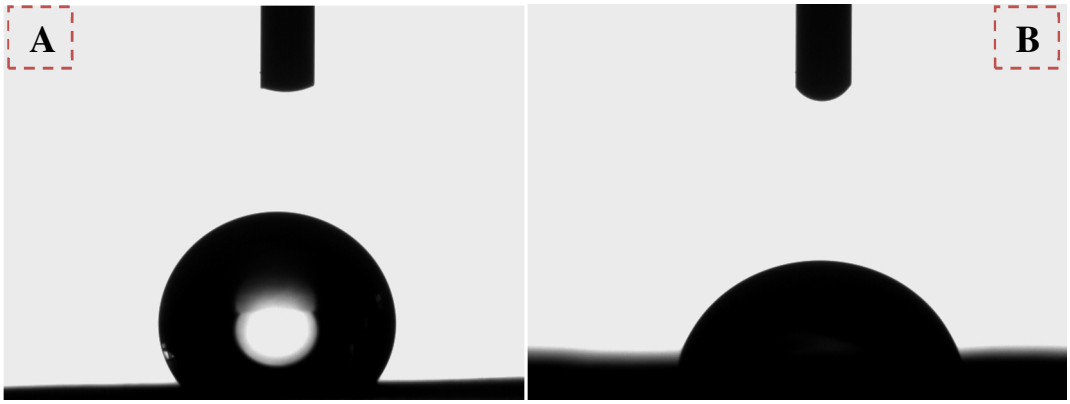

Fig. 4(A) Contact angle of water droplet on the pristine AC and ACTNF10% (B) electrodes

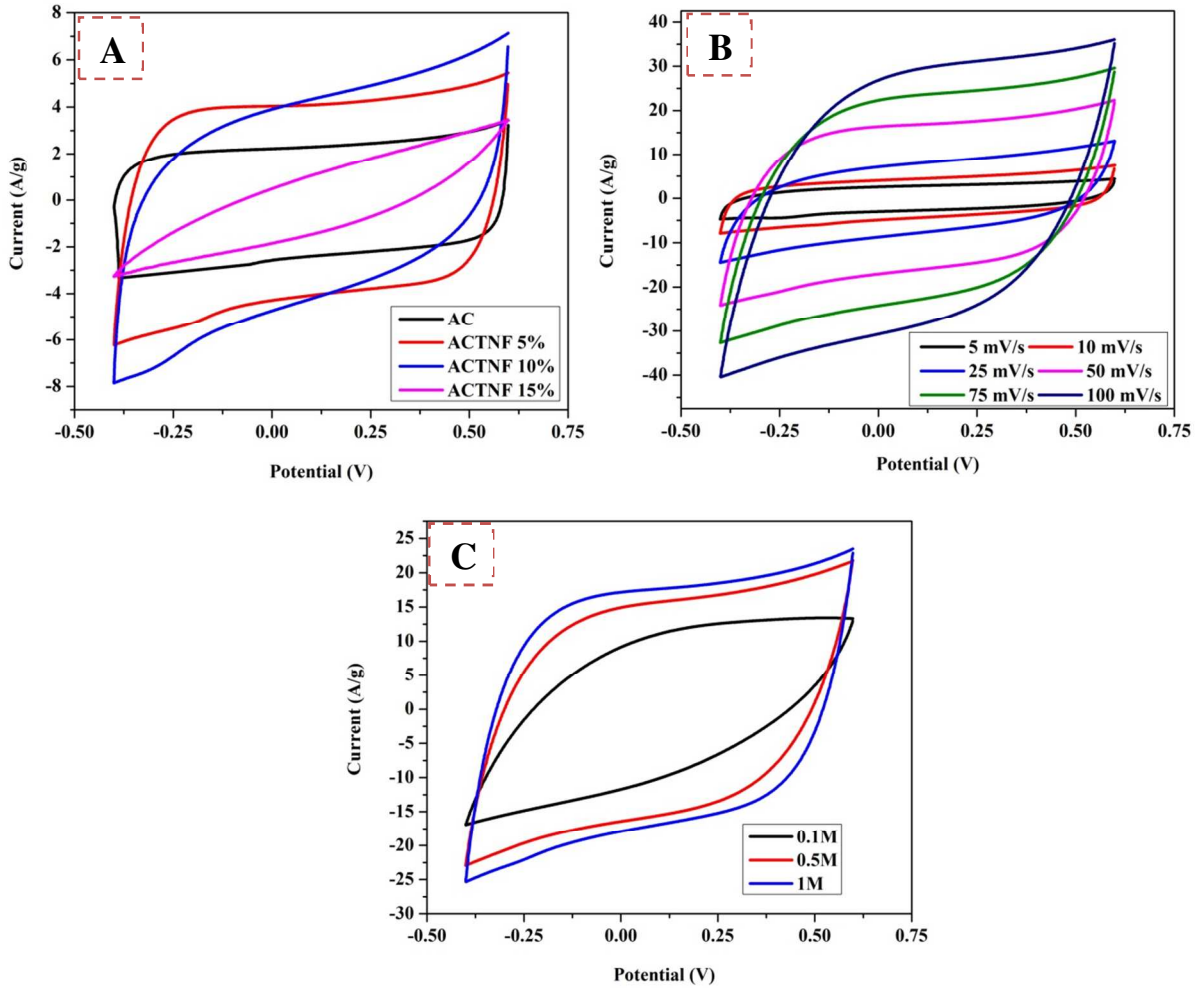

Fig. 5 (A) Cyclic voltammetry curves for the fabricated materials at a scan rate of 10 mV/s in 1 M NaCl concentration, (B) CV profiles of the ACTNF 10% at different scan rates in 1 M NaCl concentration and (C) comparison CV plot for the ACTNF 10% at a scan rate of 50 mV/s and NaCl concentrations of 0.1, 0.5 and 1 M.

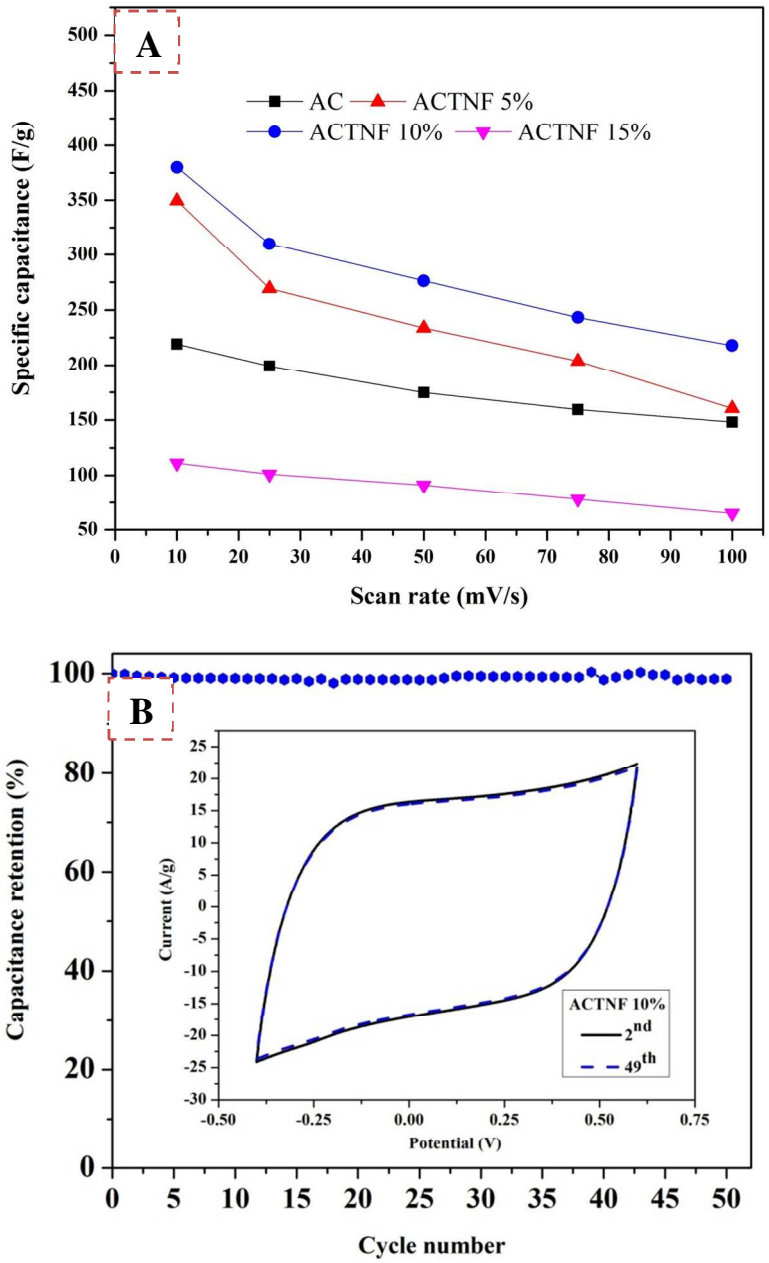

Fig. 6 (A) Specific capacitances for the prepared materials in 1 M NaCl solution at different sweep rates and capacitance retention of the ACTNF 10% electrode, the inset is comparative CV (B).

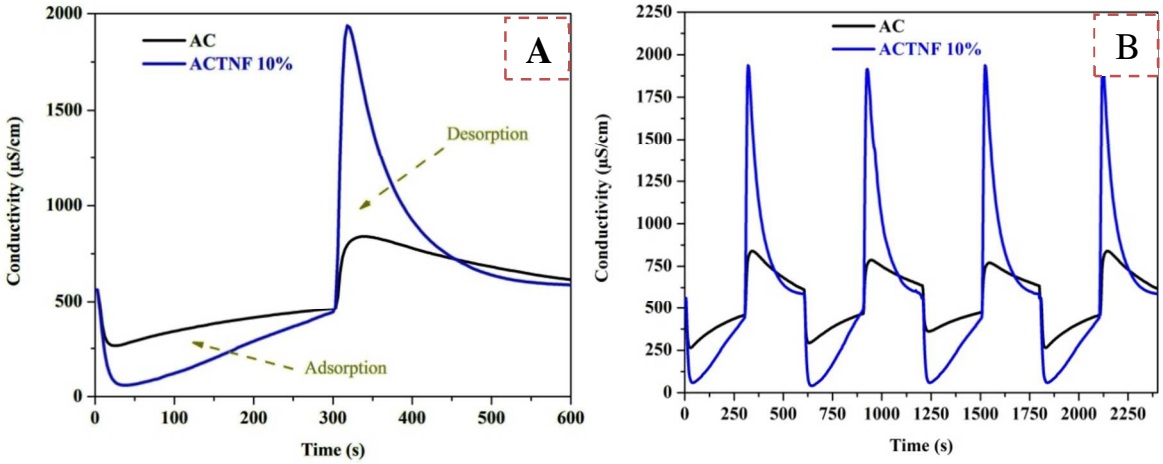

Fig. 7 (A) Desalination performance and (B) regeneration plot for the ACTNF 10% hybrid networks electrode and pristine AC under cell potential of 1.2V in 5 mM NaCl solution with flow rate of 20 mL/min.

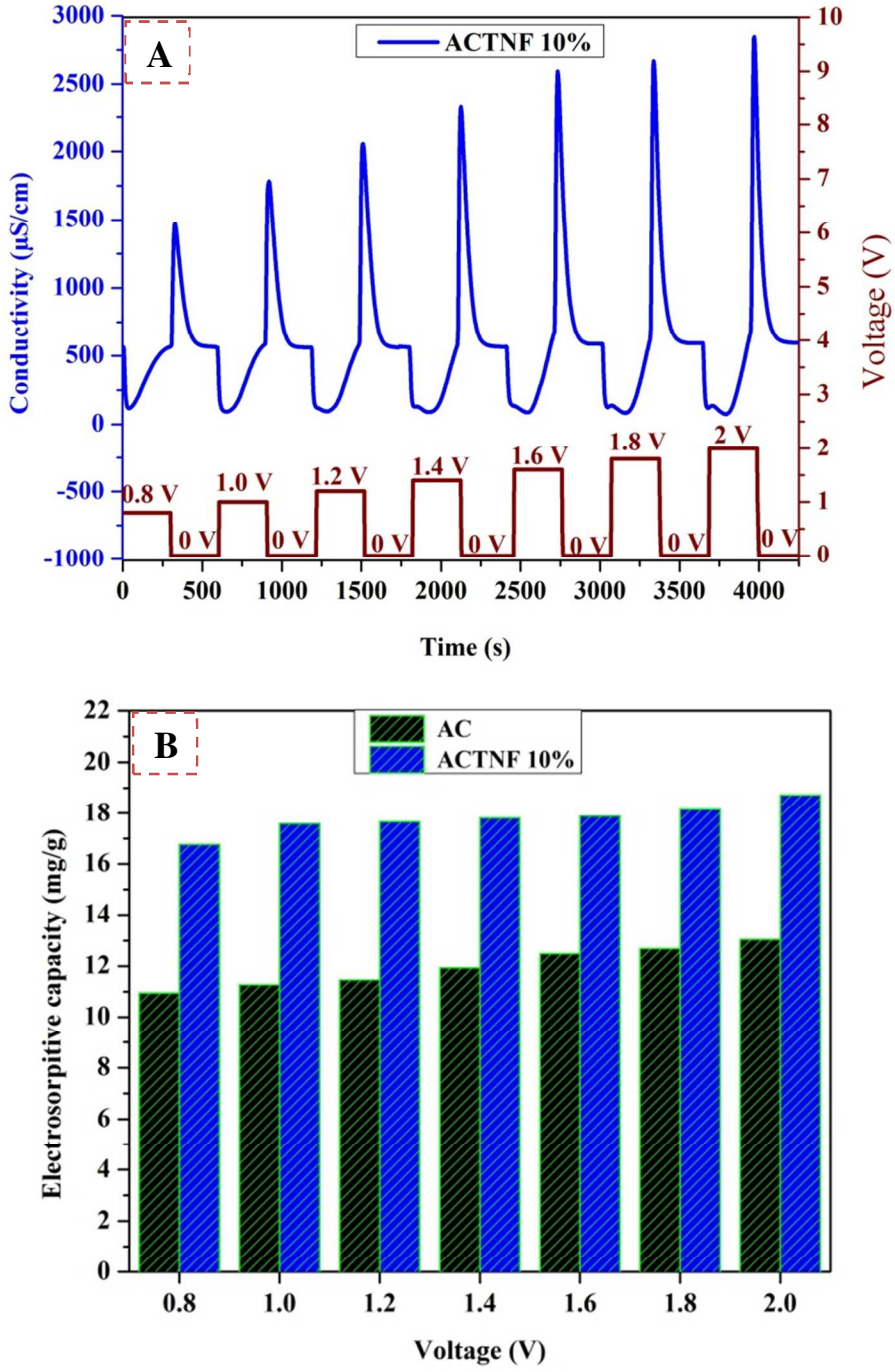

Fig. 8 (A) CDI profile versus cell potential and (B) electrosorption capacity of the pristine AC and ACTNF 10% networks electrode under different cell potential.

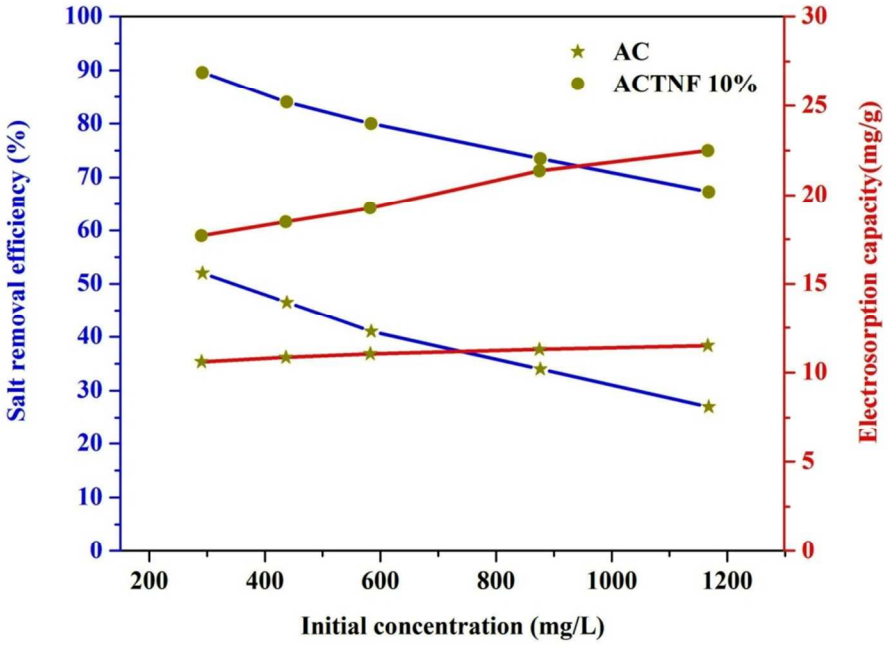

Fig. 9 Salt removal efficiency and electrosorption capacity for the pristine AC and ACTNF 10% hybrid electrode in different initial concentration under applied voltage of 1.2V.

Materials	Initial NaCl concentration (mg/L)	Cell voltage (V)	Electrosorption capacity (mg/g $_{carbon}$)	Salt removal efficiency%	Operational mode	Reference
TiO_2NPs/AC	100	1.2	~8.04	13%	BM CDI	37
TiO_2/AC	500	2	~4.75	58%	BM CDI	50
TiO_2/AC	500	1.3	3.8	30%	BM CDI	51
AC/TiO_2 spray	~584	1.2	17	35%	SP CDI	38
AC/TiO_2 NPs	500	1.2	~2.7	---	BM CDI	52
AC/TiO_2 NPs	1000	1.2	~3.1	---	BM CDI	52
ACTNF 10%	292	1.2	**17.7**	**89.6%**	SP CDI	The present work
ACTNF 10%	584	1.2	**19.26**	**80%**	SP CDI	The present work
ACTNF 10%	876	1.2	**21.73**	**73.5%**	SP CDI	The present work

Table 1 Comparison of desalination performances for different AC/TiO_2 recently published CDI electrode. SP: single-pass; BM: batch model.